Tuning stability of titania-supported Fischer-Tropsch catalysts
Impact of surface area and noble metal promotion

van Koppen, Luke M.; Dugulan, A. Iulian; Hensen, Emiel J.M.; Bezemer, G. Leendert

DOI
10.1016/j.cattod.2023.114471

Publication date
2024

Document Version
Final published version

Published in
Catalysis Today

Catalysis Today 429 (2024) 114471

Contents lists available at ScienceDirect

Catalysis Today

journal homepage: www.elsevier.com/locate/cattod

Tuning stability of titania-supported Fischer-Tropsch catalysts: Impact of surface area and noble metal promotion

Luke M. van Koppen [a,b], A. Iulian Dugulan [b], Emiel J.M. Hensen [a], G. Leendert Bezemer [c,*]

[a] Laboratory of Inorganic Materials and Catalysis, Department of Chemical Engineering and Chemistry, Eindhoven University of Technology, Het Kranenveld 14 5600 MB, Eindhoven, the Netherlands
[b] Laboratory of Fundamentals Aspects of Materials and Energy, Department of Radiation Science & Technology, Delft University of Technology, Mekelweg 15, 2628 CD, Delft, the Netherlands
[c] Energy Transition Campus Amsterdam, Shell Global Solutions International B.V., Grasweg 31, 1031 HW, Amsterdam, the Netherlands

ARTICLE INFO

Keywords:
Fischer-Tropsch synthesis
Cobalt
Oxidation
Deactivation
Mössbauer spectroscopy, SMSI

ABSTRACT

Cobalt oxidation is a relevant deactivation pathway of titania-supported cobalt catalysts used in Fischer-Tropsch synthesis (FTS). To work towards more stable catalysts, we studied the effect of the surface area of the titania support and noble metal promotion on cobalt oxidation under simulated high conversion conditions. Mössbauer spectroscopy was used to follow the evolution of cobalt during reduction and FTS operation as a function of the steam pressure. The reduction of the oxidic cobalt precursor becomes more difficult due to stronger metal-support interactions when the titania surface area is increased. The reducibility was so low for cobalt on GP350 titania (surface area 283 m^2/g) that the catalytical activity was negligible. Although cobalt was more difficult to reduce on P90 titania (94 m^2/g) than on commonly used P25 titania (50 m^2/g), the Co/P90 catalyst showed increased resistance against cobalt sintering and higher FTS performance than Co/P25. The addition of platinum to Co/P90 led to a higher reduction degree of cobalt and a higher cobalt dispersion, representing a catalyst with promising performance at relatively low steam pressure. Nevertheless, the stronger cobalt-titania interactions result in more extensive deactivation at high steam pressure due to oxidation.

1. Introduction

Fischer-Tropsch synthesis (FTS) is the reaction of synthesis gas (syngas), a mixture of CO and H_2, to long-chain hydrocarbons and other useful chemicals [1]. Since syngas can also be derived from renewable sources [2,3], FTS is a promising alternative for producing transportation fuels for sectors that are hard to decarbonize, such as heavy-duty transport and aviation. As with most industrial chemical processes, FTS utilizes a catalyst to improve the kinetics and selectivity of the reaction [4]. Commercially, iron [5] and cobalt [6] are used as the active phase for the FTS reaction. Cobalt FTS provides excellent selectivity towards long-chain hydrocarbons and is the preferred catalyst for processing of syngas derived from natural gas [7,8]. Moreover, in future Power-to-Liquid (PTL) scenarios, cobalt is also the catalyst of choice, due to its low CO_2 production, low oxygenate selectivity, that is lost to the water stream, and excellent selectivity to C_{5+} hydrocarbons [9]. Efficient catalysts require relatively large cobalt particles due to the structure sensitivity effect [10,11]. An important aspect of practical FTS is the deactivation suffered by cobalt-containing catalysts [12]. Given the high price of cobalt, it is very important to not only understand the mechanisms underlying deactivation of such catalysts but also improve catalyst formulations to mitigate deactivation [13]..

In general, the following main deactivation pathways can be discerned in cobalt-based FTS, namely (i) poisoning, (ii) carbon effects, (iii) sintering, (iv) oxidation and (v) strong metal-support interactions (SMSI) [12]. Typical poisoning agents are sulfur [14] and nitrogen compounds [15,16], while alkali metals can also reduce the performance significantly [17], [18]. Careful cleaning of the syngas feed avoids most of such poisoning problems. Instead, carbon effects, sintering, oxidation and SMSI are intrinsic to the FTS reaction and, therefore, depend on the catalyst structure and composition as well as the experimental conditions. To improve future catalyst design, these deactivation mechanisms and the extent to which they contribute will need to be fully understood. For this reason, in situ and *operando* characterization, studying catalysts in their actual working state, is of utmost importance [19].

* Corresponding author.
E-mail address: leendert.bezemer@shell.com (G.L. Bezemer).

https://doi.org/10.1016/j.cattod.2023.114471
Received 12 June 2023; Received in revised form 14 November 2023; Accepted 21 November 2023
Available online 28 November 2023

The high partial pressures of CO and surface coverage with carbon species can have two distinctive effects. First, carbon species can block access to the active sites. Although FTS is generally considered to be a reaction that does not produce coke [20], the formation of carbonaceous products with a low hydrogen content has been argued to contribute to catalyst deactivation [21]. Selective blockage of some of the active sites has been shown to enhance FTS selectivity [22,23]. Second, the presence of carbon atoms at the surface can also lead to the formation of cobalt carbides, either surface or bulk carbides, which are much less active than metallic cobalt and have different selectivity profiles [24].

Sintering of cobalt-based FTS catalysts is the result of many factors such as the relatively high operating temperature close to the Hüttig temperature of cobalt [25], the exothermicity of the reaction, and high partial pressures of steam at practical CO conversion levels [14]. Previous studies have pointed out the synergistic effect between carbon monoxide and steam towards cobalt sintering [26–28]. Both coalescence due to particle migration [29] and Ostwald ripening [30,31] through migration of cobalt atoms have been suggested as important sintering mechanisms.

The formation of large amounts of water by-product can also cause the oxidation of the surface of cobalt metal particles. Thermodynamic studies have shown that bulk oxidation of metallic cobalt particles is only favorable when the particles are smaller than 4 nm under realistic FTS conditions [32]. However, experimental studies have demonstrated that supported cobalt particles can be oxidized in the presence of co-fed water [33–36]. As such, surface and bulk oxidation of cobalt needs to be considered as a relevant deactivation mechanism.

Deactivation through strong metal-support interactions (SMSI) is obviously strongly dependent on the support material. On carbon-based supports, often used as model systems, no deactivation through SMSI is observed [27,28,37,38,39]. However, deactivation is apparent when metal oxide supports are used. Typical support materials used for the FTS reaction are irreducible oxides, such as SiO_2 [40–47] and Al_2O_3 [26,31,47–55], while a reducible oxide such as TiO_2 is also of practical interest [29,36,47,56–61]. Whilst these support materials have the benefit of anchoring the cobalt more strongly than for instance carbon, this stronger interaction can also lead to the formation of metal-support compounds (MSC) under FTS conditions [62–66].

In this work, we investigate the effect of titania as a support material for cobalt nanoparticles under humid FTS conditions that simulate high CO conversion. We vary the surface area of titania and study the impact of platinum as a reduction promoter for the optimum titania to counter possible oxidation during humid FTS operation. The chemical state and structure of cobalt is investigated under conditions close to those encountered in industrial practice using in situ Mössbauer emission spectroscopy (MES) [67]. We expand on a previous ^{57}Co MES study in which we showed how steam can lead to oxidation and sintering of cobalt nanoparticles on P25 titania [34]. The MES measurements are supplemented by XRD, *quasi* in situ XPS, CO IR Spectroscopy, TEM and STEM-EDX. The catalytic performance was measured during MES and, separately, in a fixed-bed microflow reactor.

2. Experimental methods

2.1. Catalyst preparation

Supported cobalt catalysts were prepared by incipient wetness impregnation of P25 titania (Evonik Degussa, pore volume 0.3 mL/g, BET surface area 50 m^2/g, Anatase/Rutile 85:15), P90 titania (Evonik Degussa, BET surface area 94 m^2/g), and GP350 titania (Cristal Activ™, Millennium Chemicals, BET surface area 283 m^2/g, phase-pure anatase) followed by drying in air at 120 °C for 6 h. The impregnation solutions were obtained by dissolving the appropriate amount of $Co(NO_3)_2.6\ H_2O$ (≥98.0%, Sigma Aldrich) in dehydrated ethanol and, when required, an appropriate amount of $Pt(NH_3)_4(NO_3)_2$ (≥99.995%, Sigma Aldrich). A total of four catalysts were prepared with a cobalt loading of 4 wt%. One catalyst was promoted with platinum at an atomic cobalt/platinum ratio of 200. The resulting samples are denoted by CoPt/S and Co/S for the promoted and unpromoted catalysts respectively, where S stands for the support being P25, P90 or GP350. For Mössbauer emissions spectroscopy measurements, a portion of the dried catalysts was spiked with radioactive ^{57}Co by pore volume impregnation using a solution containing 90 MBq ^{57}Co in 0.1 M HNO_3. These radioactive samples were dried at 120 °C for 12 h.

2.2. Characterization

2.2.1. X-ray diffraction

X-ray diffraction (XRD) patterns were recorded following the same procedure as reported previously [36]. Briefly, XRD patterns were obtained on a Bruker D2 Phaser using a Cu Kα radiation source and a 2 mm slit (time per step 0.15 min; step size 0.1° in the 2θ range of 10–60°). the Bruker Diffrac.Eva software was used for data analysis.

2.2.2. Electron microscopy

To determine the cobalt particle size and its distribution, transmission electron microscopy (TEM, FEI Tecnai 20, 200 kV, LaB6) and scanning transmission electron microscopy-energy-dispersive X-ray spectroscopy (STEM-EDX, FEI cubed Cs-corrected Titan, 300 kV, FEG) measurements were carried out. For these measurements, the sample was ground, suspended in ethanol and dispersed on a holey carbon film held by a Cu grid. The average size and size distribution of the particles were determined from TEM images. The nanoscale distribution of the elements was determined by STEM-EDX. Elemental analysis was performed by an Oxford Instruments EDX detector (X-MaxN-100TLE).

2.2.3. Quasi in situ X-ray photoelectron spectroscopy (XPS)

The oxidation state of cobalt was studied by *quasi* in situ XPS using a Kratos AXIS Ultra 600 spectrometer equipped with a monochromatic Al Kα X-ray source (Al Kα 1486.6 eV). Survey and region scans were obtained at pass energies of 160 and 40 eV, respectively, with a step size of 0.1 eV. The background pressure in the XPS was below 10^{-9} mbar. Sample pre-treatment was done in a high-temperature reaction cell (Kratos, WX-530) attached to the XPS analysis chamber. This setup allows in vacuo transfer of a pre-treated sample into the XPS analysis chamber. Reduction treatments were performed in a pure H_2 flow at atmospheric pressure and temperatures between 340 and 650 °C. After

Table 1
Average metal oxide particle size, Co/Ti ratio, and reducibility of $Co(Pt)/TiO_2$ catalysts.

Catalyst	Co/Ti (calcined)[a]	Reduction temperature (°C)	Co/Ti (reduced)[a]	DOR (%)[b]	Cobalt particle size (nm)[c]
Co/P25	0.163	340	0.041	43	13.4 ± 6.6
Co/P90	0.062	340	0.029	28	8.0 ± 3.4
Co/GP350	0.034	340	0.024	3	4.6 ± 2.6

[a] Atomic Co/Ti ratio determined by XPS,
[b] Degree of reduction determined by XPS.
[c] Determined by TEM analysis of reduced and passivated samples.

pre-treatment, the cell was evacuated to a pressure lower than 10^{-9} mbar. When the sample temperature was below 150 °C, it was transferred to the XPS analysis chamber. Data analysis was done with the CasaXPS software (version 2.3.22PR1.0). The binding energy scale was corrected for surface charging by setting the binding energy of the Ti $2p_{3/2}$ peak of TiO_2 to 458.5 eV.

2.2.4. In situ Mössbauer emission spectroscopy

Mössbauer emission spectroscopy (MES) was carried out at various temperatures using a constant acceleration spectrometer set up in a triangular mode with a moving single-line $K_4Fe(CN)_6{\cdot}3\ H_2O$ absorber enriched in ^{57}Fe. Further details about this setup ared described in the literature [28]. Measurements under Fischer-Tropsch conditions were carried out in a high-pressure MES cell [67], which is also described in detail in the literature [28].

The MossWinn 4.0 software was used to fit the Mössbauer [68]. Very small metallic superparamagnetic species were modeled using the two-state magnetic relaxation model of Blume and Tjon, assuming a a fluctuating magnetic field that jumps between +H and -H along the z-axis with an average frequency τ [69]. A typical value of H is 500 kOe, while τ can vary between 10^{-9} and 10^{-12} s^{-1}. Larger metallic particles were fitted with a hyperfine sextuplet, while doublets were used to describe oxidic contributions, the quadrupole splitting indicating the non-spherical charge distribution. The experimental uncertainties in the calculated Mössbauer parameters were estimated using Monte Carlo iterations within MossWinn 4.0. Including experimental uncertainties, these uncertainties were as follows: IS and QS ± 0.01 mm s^{-1} for the isomer shift and quadrupole splitting, respectively; ± 3% for the spectral contribution; ± 3 kOe for the hyperfine field.

In a typical experiment, 300 mg of ^{57}Co-spiked and 100 mg of non-radioactive catalyst (sieve fraction 250–500 μm) was loaded into two separate compartments of the reactor cell. FTS experiments were performed following reduction between 340 °C and 400 °C for 2 h in a 100 mL/min flow of pure H_2. Reactions were done at 200 °C and 20 bar, while the H_2/CO was kept at 4 throughout and steam was fed to vary the relative humidity. Relative humidity values are reported based on added steam only. Further details about the feed ana analysis section can be found in the literature [28].

2.3. Catalytic activity measurements

The catalytic performance was determined in a single-pass flow reactor system (Microactivity Reference unit, PID Eng&Tech. In a typical experiment, 50 mg of catalyst (sieve fraction 125–250 μm) was mixed with same-sized SiC to a total volume of 3 mL and placed in a tubular reactor with an internal diameter of 9 mm. Reduction was performed in flowing H_2 at 340 °C for 2 h after heating at a rate of 5 °C/min. The catalytic performance was evaluated at 220 °C or 240 °C, a total pressure of 20 bar and a H_2/CO ratio of 4 at a space velocity (SV) of 60 L g_{cat}^{-1} h^{-1}. The CO conversion (X_{CO}) -which ranged between 1% and 5%- was determined in the following manner:

$$X_{CO} = 1 - \frac{F_{Ar,in}F_{CO,out}}{F_{CO,in}F_{Ar,out}} \quad (1)$$

where $F_{Ar,in}$ is the molar Ar flow in the reactor feed, $F_{CO,in}$ is the molar CO flow in the reactor feed, $F_{Ar,out}$ and $F_{CO,out}$ are the respective molar flows of Ar and CO out of the reactor system. Due to the use of Ar as the internal standard, $F_{Ar,in}/F_{CO,in}$ can be measured and calibrated in a blank experiment.

The carbon-based selectivity of hydrocarbon compound C_i (S_{Ci}) was calculated using:

$$S_{Ci} = \frac{F_{Ar,in}F_{Ci}v_i}{F_{Ar,out}F_{CO,in}X_{CO}} \quad (2)$$

where F_{Ci} is the molar flow of hydrocarbon compound C_i out of the reactor, and v_i is the stochiometric factor of the hydrocarbon compound.

The cobalt time-yield (CTY) was determined using the following equation:

$$CTY = \frac{F_{CO,in}X_{CO}}{m_{Co}} \quad (3)$$

where m_{Co} is the weight of cobalt loaded in the reactor.

3. Results and discussion

3.1. Characterization of titania-supported catalysts

A set of three Co/TiO_2 catalysts without Pt reduction promoter was prepared by incipient wetness impregnation at a cobalt loading of 4 wt% using different titania supports covering surface areas in the range of 50 – 283 m^2/g. The X-ray diffractograms of the calcined precursors are given in Fig. S12. The samples show only diffraction lines due to anatase and rutile TiO_2, which is expected for catalysts based on P25 [70] and P90 [71] TiO_2. The catalyst based on GP350 only contains anatase according to XRD analysis as per specifications. The absence of diffraction lines due to cobalt oxide points to the high dispersion of the cobalt oxide precursor.

Fig. 1 shows representative TEM images of the catalysts after reduction at 340 °C for 2 h in pure H_2 and subsequent passivation at room temperature in a flow of 5% O_2 in He. The images show the clear difference between the structure of the more conventional P25 and P90 supports and the GP350 support. The GP350 support is obtained by hydrolysis of titanium oxychloride [72], resulting in anatase particles smaller than 10 nm, which agglomerate to form flower-like clusters as can be seen in the TEM images. This high-surface-area titania is thus prepared in a different way than the flame synthesized P25 and P90 supports that are produced from $TiCl_4$. Importantly, all three titania samples were prepared via a non-sulfate route, implying that the samples are free from sulfur, which is a known FTS poison. The average size and size distribution of the cobalt nanoparticles was determined by analyzing approximately 150 particles in ca. 8 images per sample. On average, the cobalt particle size decreases from 13.4 nm for Co/P25 to 8.0 nm for Co/P90 and 4.6 nm for Co/GP350, indicating that smaller cobalt particles are obtained with increasing surface area of the titania support. Since the pore size of the support is inversely proportional to the surface area, this decrease in apparent cobalt particle size could be attributed to a pore size effect previously shown by van Steen et al. on silica and alumina [71]. However, this effect was observed on catalysts prepared with high cobalt content (14–20 wt%), whereas we used a much lower loading of 4 wt%, resulting in particles much smaller than the pore size of the support. The TEM images show that the cobalt phase is well dispersed over the surface without any large agglomerates of cobalt. The contrast differences between the various catalysts may suggest a lower cobalt reduction degree, which is most evident by comparing Co/GP350 to Co/P25.

The surface of the catalysts was characterized using *quasi* in situ XPS. Survey scans revealed no contributions from unexpected elements on any of the measured samples, as such the presence of alkali metals and sulfur on the catalyst surface were excluded. The Co $2p_{3/2}$ spectra of the calcined catalysts and the catalysts reduced at 340 °C catalysts are given in Fig. 2. Fitting was done using the model of Biesinger et al. [73]. Additional spectra obtained at higher reduction temperatures can be found in Fig. S6. The atomic ratio of cobalt to titanium (Co/Ti ratio) of the oxidic precursors decreases as expected with the increasing surface area of the titania support and is consistent with the expected decrease by a factor of two for P90 compared to P25, and by a factor of five for GP350. During reduction, the differences in the Co/Ti ratios become much smaller, suggesting agglomeration of the cobalt phase during the reduction of cobalt oxide to metallic cobalt [36,74]. Titania overlayer formation can also explain this, which has previously been observed

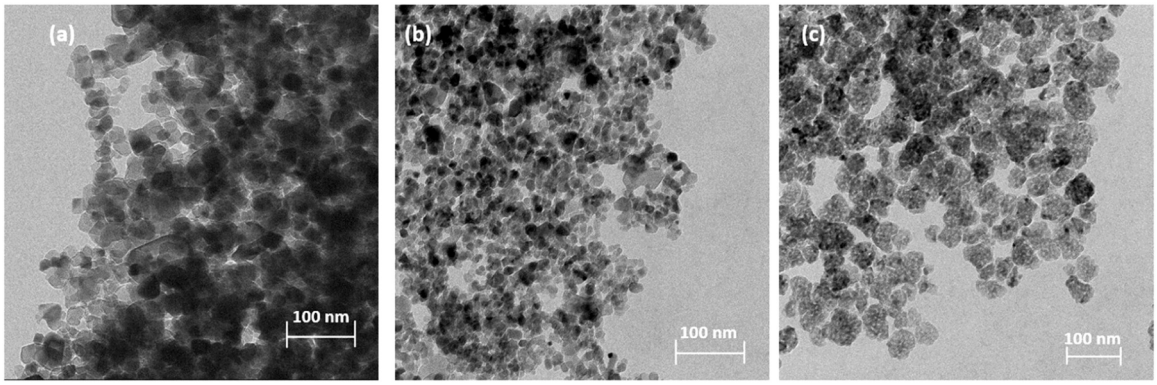

Fig. 1. Representative TEM images of (a) Co/P25, (b) Co/P90, and (c) Co/GP350 following reduction at 340 °C for 2 h and passivation in 5% O_2 in He at room temperature.

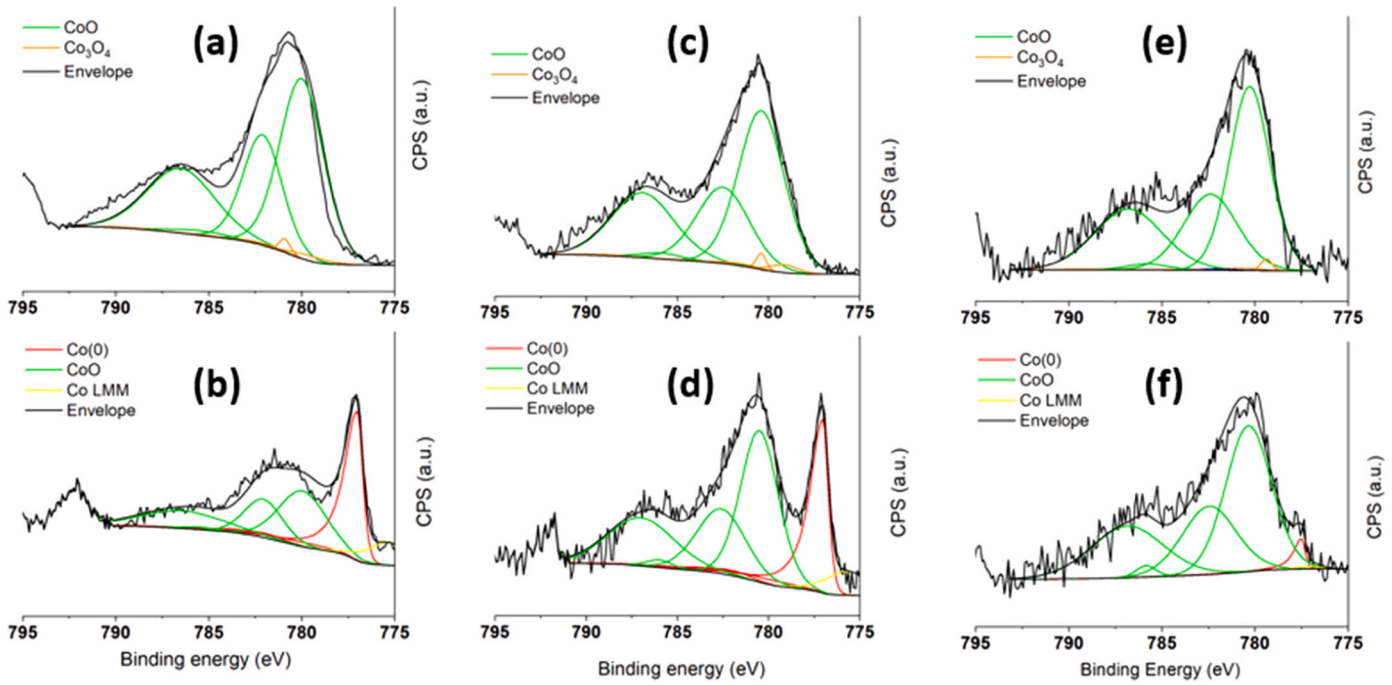

Fig. 2. Co $2p_{3/2}$ XPS spectra of Co/P25 (a,b), Co/P90 (c,d), and Co/GP350 (e,f) after (a,c,e) calcination and (b,d,f) subsequent reduction at 340 °C (black: experimental data and the fitted envelope; red: the fitted metallic Co(0) contributions; green: the fitted CoO contributions; orange: fitted Co_3O_4 contributions; yellow: the Co auger LMM peak).

under reducing conditions and can be especially relevant for high surface area titania supports [29]. The decrease in the Co/Ti ratio is most pronounced for Co/P25 and least for Co/GP350. The contribution of metallic cobalt as determined by fitting of the Co $2p_{3/2}$ spectra was used to calculate the degree of reduction (DOR). The DOR of Co/P25 amounts to 43% after reduction at 340 °C. While the DOR for Co/P90 is significantly lower at 28%, only a very small amount of cobalt is reduced in Co/GP350 according to XPS. These findings clearly demonstrate that the cobalt oxide reducibility is significantly more difficult when the cobalt-titania interactions become stronger due to the higher surface area of the titania support [47]. We speculate that the reduction of cobalt oxide will lead to significantly larger metallic cobalt particles due to sintering as observed for Co/P25. The much smaller particles observed in Co/GP350 after reduction at 340 °C are likely cobalt oxide particles, as suggested by the very low DOR of 3% according to XPS. We also reduced the Co/P90 and Co/GP350 catalysts at higher temperatures. These results are discussed in the SI (Table S7, Fig. S8-S9).

3.1.1. *In situ* Mössbauer spectroscopy of reduced catalysts

Mössbauer spectra of the catalysts after reduction at 340 °C for 2 h are given in Fig. 3a. The Mössbauer fit parameters of the reduced catalysts are listed in Tables S2-S4. The sextuplet with an isomer shift (I.S.) of − 0.1 mm s^{-1} and a hyperfine field (H.F.) of ~323 kOe observed for all catalyst samples is due to metallic cobalt. This contribution comes from magnetically ordered metallic cobalt particles, which is common for cobalt particles larger than 6 nm [27]. The absence of a singlet indicates that these samples do not contain superparamagnetic cobalt, meaning that all metallic cobalt particles are larger than 6 nm. This implies that a significant part of the small cobalt particles seen by TEM are oxidic in nature, which is consistent with the substantial contribution of a dispersed Co^{2+}-oxide phase in the MES spectra as represented by a doublet with an I.S. of 1.0 mm s^{-1} and a quadrupole splitting (Q.S.) of 2.0 mm s^{-1} [75]. The contribution of cobalt oxide is significantly higher for Co/P90 and Co/GP350 than for Co/P25. The latter sample shows a nearly complete reduction of cobalt, while the reduction degree in the other two samples is about half. The DOR values according to MES

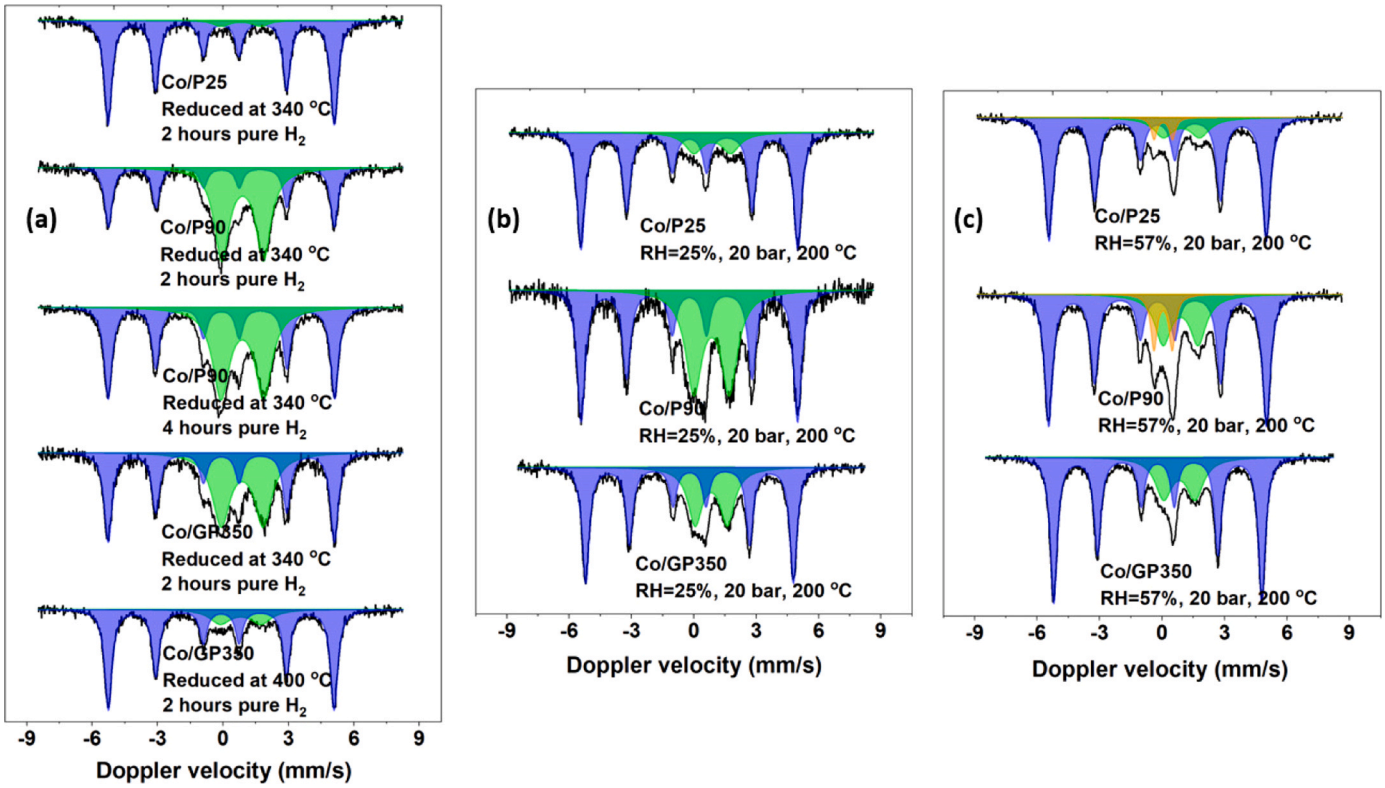

Fig. 3. In situ Mössbauer spectra of the Co/TiO_2 catalysts (a) following reduction, and under FTS conditions at a relative humidity of (b) 25%, and (c) 57%. The black lines represent the experimental spectra, the blue ones the fitted bulk metallic cobalt sextuplet, and the orange and green ones the fitted oxidic cobalt doublets.

after reduction at 340 °C are significantly higher than those according to XPS analysis. A tentative explanation for this discrepancy can be found in the size of the metallic and oxidic cobalt particles. As observed for Co/P25 and for other typical Co on titania catalysts [36,74], substantial sintering of cobalt takes place during the reduction to the metallic phase. For instance, the metallic cobalt particles in reduced Co/P25 are significantly larger than 10 nm. Given that the inelastic mean free path of cobalt 2p electrons is in the range of 1–2 nm in the XPS experiment, only a small fraction of the cobalt atoms in metallic cobalt particles are probed. As the cobalt oxide particles are much smaller due to the strong interactions with titania, it is likely that a larger fraction of the cobalt oxide phase is probed by XPS. In principle, Mössbauer spectroscopy probes all Co nuclei, being more representative for the overall reduction degree of cobalt. This line of reasoning can explain the discrepancies in the DOR noted here between MES and XPS. While XPS shows a DOR for Co/P25 of 43%, the DOR according to MES is 95%. The DOR according to XPS and MES for Co/P90 are respectively 28% and 40%. The largest difference in DOR as probed by XPS and MES is for Co/GP350 with respective values of 3% and 54%. This could imply the presence of a few very large metallic cobalt particles, which is not clearly supported by the MES hyperfine field nor the TEM analysis. A possible alternative explanation might be that the metallic cobalt phase is partially covered by titanium, decreasing effectively the XPS signal. The formation of such titania layers on cobalt has been reported for P25 titania [29,58]. Recent work showed the formation of TiO_x bilayers on Ni particles in Ni/TiO_2 during reduction at 400 °C [76]. Such effects may be expected to be even stronger for the Co/GP350 catalyst, given its much higher surface area. Moreover, Wolf et al. reported that cobalt tends to form more metal-support compounds with phase-pure anatase [66], which suggests that not only the surface area but also the chemistry of the GP350 support increase the cobalt-titania interaction. As cobalt was not fully reduced for Co/P90 and Co/GP350 in the first step, additional reduction treatments were applied. First, the reduction time was extended by 2 h at 340 °C, which only marginally improved the DOR for both catalysts, i.e., from 40% to 49% for Co/P90 and from 54% to 59% on the GP350 support. Afterwards, an additional 2-hour reduction at 400 °C for GP350 further increased the DOR to 84%. Despite these differences, the spectral parameters of the metallic cobalt phase following their final reduction are the same for all samples, indicating that the metallic cobalt particles are not too different in size.

3.2. *In situ Mössbauer emission spectroscopy during the FTS reaction*

In situ Mössbauer emission spectra were recorded as a function of the steam partial pressure at a temperature of 200 °C, a total pressure of 20 bar, and a H_2/CO ratio of 4. The steam content in the feed is expressed as the relative humidity (RH) at the applied conditions. Table S1 details the feed compositions for the different RH measurements. Spectra were recorded for at least 48 h at each humidity step, except for RHs of 25% and 57% where the steam treatment was prolonged to 5 days and 11 days, respectively. This was done to understand the influence of prolonged exposure as encountered in industrial practice. Under dry FTS conditions (RH = 0%) measured at 200 °C, the metallic cobalt contribution of Co/P25 remained the same as after initial reduction. In contrast, the metallic contribution for Co/P90 increased from 49% after reduction to 64% during dry FTS conditions, as can be seen in Table 2. This increase of metallic cobalt at 200 °C can be caused by two effects, it is partially the result of a difference in Debye temperature of the metallic and oxidic cobalt phases [77], but it is also due to improved reducibility under the mildly reducing FTS conditions. This is evident from the measurement performed at room temperature following the dry FTS conditions given in Table S3, which showed an increase to 58% metallic cobalt compared to 49% for the freshly reduced catalyst.

The catalytic activity of the Co/GP350 catalyst was negligible under the initial dry FTS conditions. For that reason, an extra reduction step at 400 °C was performed, which resulted in a metallic cobalt contribution of 84% when measured at room temperature and 81% when measured at

Table 2
Contribution of the different cobalt phases as determined from MES spectra recorded at 200 °C under varying FTS conditions.

Treatment	H_2O/H_2	Spectral contribution cobalt (%)					
		Co/P25		Co/P90		Co/GP350	
		Co^0	Co-oxide	Co (0)	Co-oxide	Co (0)	Co-oxide
Reduced[a]	0	95	5	49	51	84	-
RH 0%	0	95	5	64	36	81	19
RH 7.5%	0.25	87	13	60	40	73	27
RH 14%	0.50	86	14	58	42	66	24
RH 20%	0.75	86	14	57	43	66	24
RH 25%	1.0	84	16	56	44	67	23
Reduced[a]	0	95	5	79	21	76	24
RH 0%	0	91	9	74	26	78	22
RH 57%	1.0	80	15 / 5	65	24 / 11	75	25

[a] Reduced spectra were recorded at room temperature.

200 °C. However, this additional reduction step did not increase the activity. These findings are most likely due to the formation of titania overlayers, as discussed above. Thus, even though the reduction degree can be as high as 84%, blocking of the active sites by SMSI leads to very low activity.

Following dry FTS conditions, the humidity was increased during the MES measurements. The evolution of the metallic cobalt contribution is given in Table 2. Fig. 3b shows the MES spectra for the catalyst at RH = 25%, demonstrating a gradual shift from bulk metallic cobalt to oxidic cobalt for all three samples. The spectra at RH = 25% can be fitted with a bulk metallic cobalt contribution (I.S. = −0.2 mm s^{-1}, H.F. in the 308–310 kOe) and an oxidic cobalt contribution (I.S. = 0.8 mm s^{-1}, Q.S. = 1.6–1.7 m s^{-1}). The latter spectral features of the oxidic feature represent well-dispersed Co^{2+} species, which are similar to the oxidic phase remaining in the initially reduced catalysts. Despite this, the Co/P90 sample contains significantly more oxidic cobalt than the other catalysts at RH = 25%. On the other hand, the oxidic cobalt contribution was already the highest among the three catalysts after reduction and operation under dry conditions (RH = 0%). Comparing the oxidic contributions between dry FTS and RH = 25% conditions, we can observe that operating at RH = 25% leads to more extensive oxidization of metallic cobalt in the order of Co/GP350 (from 81% to 67%) > Co/P25 (from 95% to 84%) > Co/P90 (from 64% to 56%). After treatment at RH = 25%, the catalysts were reduced again at 340 °C for 2 h. The resulting spectral parameters in Tables S2-S4 show an increase in the DOR for Co/P90 and Co/GP350 compared to the DOR after the reduction. As smaller cobalt oxide particles are typically more difficult to reduce than larger ones [47], this can be taken as an indication that the catalyst exhibit a lower dispersion after the oxidation-reduction treatment. This effect is more pronounced for the Co/P90 catalyst, for which the DOR amounted to 79% after the second reduction step in comparison to 40% after the initial one. After this intermittent reduction step, the samples were exposed to the highest humidity of RH = 57%. This led to a new oxidic cobalt contribution for the Co/P25 and Co/P90 catalysts (Fig. 3c). The spectral parameters of this phase (IS = 0.0–0.1 mm s^{-1}, QS = 0.8–0.9 mm s^{-1}) correspond to those of Co^{3+}, which is a signature of agglomerated Co^{2+} as explained in our previous work [36]. As such, the appearance of this contribution in Co/P25 and Co/P90 indicates significant sintering of cobalt in the oxide form. This less dispersed cobalt oxide phase is not observed in Co/GP350 treated at RH = 57%, despite the already large contribution of this phase. The absence of the Co^{3+} signal on GP350 is likely due to the strong interaction between cobalt and titania, limiting the mobility of the metallic and oxidic species. The formation of significant titania overlayers during reduction would further limit this mobility and explain the lack of oxidic cobalt agglomeration compared to the other catalysts. The mobility of oxidic cobalt at high RH observed here for Co/P25 and Co/P90 is consistent with the mobility observed for oxidic cobalt on P25 support [36]. Compared to the catalyst following the RH = 25% conditions, the total amount of oxide following the highest humidity is lower for the Co/P90 and Co/GP350 catalysts, as seen in Table 2, this is likely the result of the increased DOR obtained after the intermittent reduction treatment, but alternatively sintering of cobalt oxide to larger metallic particles as reported by Claeys' group [34] can also explain this finding. The latter is supported by the observation that the H.F. increased for both the P90 (308–310 kOe) and GP350 (310–311 kOe) catalysts at RH = 57% compared to RH = 25% conditions.

Fig. 4 shows the relative amount of metallic cobalt in the three titania-supported cobalt catalysts under the increasing humid conditions. The trend for the three catalysts is qualitatively similar with a gradual decrease during the first steps and a small increase at the highest humidity conditions, which is due to the reduction step after RH = 25%. This clearly shows that the increased oxidation observed does not correlate with the titania surface area. Compared to Co/P25, Co/P90 and Co/GP350 with a higher surface area exhibit a lower cobalt reducibility, which results in a higher contribution of oxidic cobalt throughout the prolonged FTS testing as a function of the humidity. Whilst the P90 support showed the highest initial contribution of cobalt oxide, this contribution did not increase as strong as for the other two catalysts. The DOR upon initial reduction was highest for Co/P25 and this catalyst was most prone to cobalt oxidation under simulated high conversion conditions. All three titania-supported cobalt catalysts show significant oxidation of cobalt (10–15%) when operating at increased steam pressure. A re-reduction is capable to restore the degree of reduction. The observation that oxidation does take place during conditions that can be reached during industrial FTS requires the design of catalysts that are capable to endure such conditions. Below, we will show results of platinum addition to improve stability, but first we will discuss used catalyst characterization.

3.3. Used catalyst characterization

The MES data were complemented by STEM-EDX measurements of reduced-passivated and used Co/P90 for comparison with STEM-EDX images of Co/P25 presented in our previous work [36]. The term 'used catalysts' refers to the non-radioactive catalyst samples obtained from the Mössbauer cell under the same humid FTS treatments as the

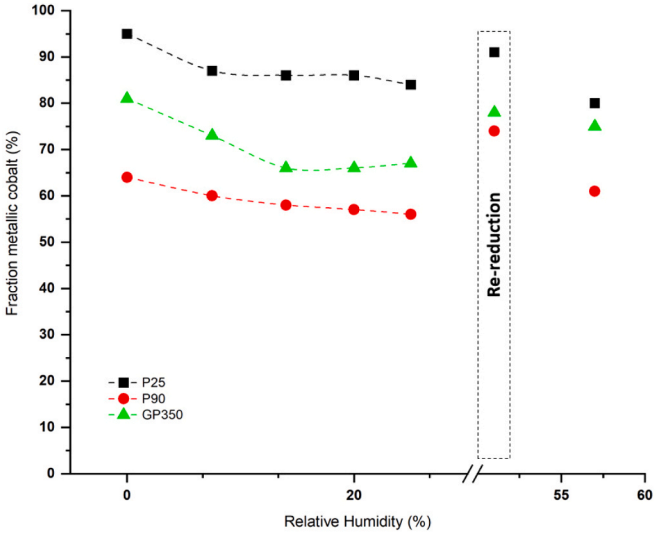

Fig. 4. Fraction of metallic cobalt in Co/TiO_2 catalysts under humid Fischer-Tropsch conditions (200 °C, 20 bar, H_2/CO = 4) as determined by Mössbauer spectroscopy at 200 °C as a function of the relative humidity. The axis break points to the reduction treatment carried out after the RH = 25% treatment and before the RH = 57% treatment (reduction in H_2, at 340 °C for 2 h). The data inside the dashed box pertain to the catalyst directly after reduction at 200 °C.

Mössbauer samples. As such, these measurements provide ex situ information about the state of the catalyst following the deactivation studies. For each sample, eight EDX maps were obtained on different areas of the sample. Two representative maps of the reduced and passivated Co/P90 are shown in Fig. 5a-b. These images show well-dispersed cobalt over the titania support, with a few larger cobalt particles around 8–12 nm.

Representative maps of the used Co/P90 catalyst following high humidity FTS are given in Fig. 5c-d. Contrary to EDX mappings performed on the P25 sample, no significant sintering is observed for this catalyst. The cobalt remains well dispersed over the titania and only a few larger cobalt particles can be seen with sizes of approximately 8–12 nm, similar to the reduced and passivated sample. This suggests that cobalt is far less mobile on this support compared to Co/P25, which can be linked to the higher surface area of P90 titania. So, although this stronger interaction with the support decreases the DOR as observed before, it also results in less sintering during FTS operation under practical high CO conversion conditions.

3.4. Platinum promotion

Since the P90 support showed promising resistance to cobalt sintering amid lower reducibility than with the convention P25 support, we studied the addition of platinum as a reduction promoter for P90 support catalysts. To this end, an identical catalyst on the P90 titania support was prepared with the only difference that platinum was added to the impregnation solution. The X-ray diffractogram of the calcined precursor is given in Fig. S12 together with that of the non-promoted catalyst. Both diffractograms only show diffraction lines belonging to anatase and rutile, as expected for the P90 support, without indications of other cobalt or platinum phases, indicative of their high dispersion.

Quasi in situ XPS spectra of the Co $2p_{3/2}$ region of calcined and reduced CoPt/P90 catalyst are given in Fig. S10. The Co/Ti ratios for the calcined and reduced catalysts as well as their DOR are given in Table S7. Compared to the platinum-free counterpart (Fig. 2), the feature due to metallic cobalt is much more pronounced, indicative of a higher DOR. This is expected, as platinum is known to act as a reduction promoter [57,78]. After reduction at 340 °C for 2 h, the DOR for CoPt/P90 is 79% according to XPS, substantially higher than the DOR of 28% for Co/P90 after the same reduction treatment. The Co/Ti ratio for the calcined precursor is significantly smaller in the presence of platinum, which may hint at a lower dispersion of the cobalt oxide phase upon calcination. Furthermore, the Co/Ti ratio of the CoPt/P90 catalyst following a reduction at 340 °C is smaller (0.019) than that found on the Co/P90 catalyst (0.029) following the same treatment. However, the platinum-promoted catalyst contains significantly more metallic cobalt at the surface, which makes a comparison challenging, since oxidic cobalt species on titania are known to sinter extensively upon reduction [36,74]. Reduction of Co/P90 at 500 °C results in a DOR comparable to the one obtained upon reduction of CoPt/P90 at 340 °C. However, reduction of Co/P90 at 500 °C leads to a lower Co/Ti of 0.007 in comparison to the value of 0.019 for CoPt/P90, implying a positive effect on the metallic cobalt dispersion due to the platinum promoter.

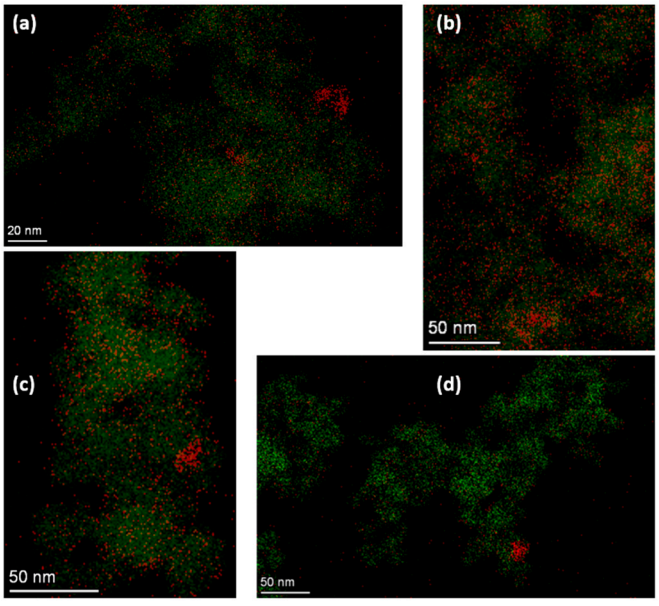

Fig. 5. EDX mappings of (a-b) a reduced and passivated Co/P90 catalyst and (c-d) a used Co/P90 catalyst: the cobalt mapping is shown in red and the titania mapping in dark green.

3.4.1. In situ Mössbauer spectroscopy of reduced catalysts

The Mössbauer spectrum of the promoted catalyst after reduction at 340 °C for 2 h is given in Fig. S6a along with the reduced spectra of the non-promoted Co/P90 catalyst. The Mössbauer fit parameters of the reduced catalyst are listed in Table S5. The reduced promoted catalyst shows a sextuplet with an I.S. of − 0.1 mm s^{-1} and an H.F. of 317 kOe, which points to magnetically ordered metallic cobalt with a size larger than 6 nm [27]. The absence of a singlet contribution shows that these large particles are the predominant metallic cobalt phase. The H.F. of the metallic particles for the platinum-promoted sample is smaller than that of the corresponding sample without platinum. This difference points to a higher dispersion of these particles in the platinum-promoted catalyst, which was also observed through XPS analysis. The platinum promoter enhances the reducibility of cobalt oxide by hydrogen spillover from metallic platinum [76]. Our results show that this results in more dispersed metallic cobalt particles. Next to the metallic phase, an oxidic contribution is observed with I.S. = 1.0 mm s^{-1} and Q.S. = 1.9 mm s^{-1}, which represents dispersed Co^{2+}-oxide, and indicates non-complete reduction. However, the DOR observed through Mössbauer for CoPt/P90 is 71%, which is significantly higher than without platinum (49%). This is in good agreement with the XPS analysis and highlights the beneficial effect of the reduction promoter.

3.5. In situ Mössbauer emission spectroscopy during the FTS reaction

In situ Mössbauer spectra were measured during FTS measurements for the platinum-promoted sample, according to the conditions given in Table S1. The platinum-promoted catalyst shows the same Mössbauer features as the non-promoted counterpart when changing from dry to RH = 25% conditions, as shown in Fig. S6b. A sextuplet is observed corresponding to bulk magnetically ordered cobalt with an I.S. of − 0.2 mm s^{-1} and a H.F. of 302 kOe for the CoPt/P90 catalyst at 200 °C. Next to the sextuplet, there is an oxidic doublet with an I.S. of 0.8 mm s^{-1} and a Q.S. of 1.6 mm s^{-1}, indicative of dispersed Co^{2+}. The first humidity steps show a gradual increase in the contribution of oxidic cobalt (Table 3), which is in the same order of magnitude as the previously measured non-promoted Co/P90 catalyst.

When the relative humidity is further increased to 57%, the promoted catalyst behaves differently from the non-promoted sample in the sense that the second oxidic cobalt doublet due to agglomerated cobalt does not appear (Fig. S6b). This suggests that the presence of platinum suppresses the mobility of oxidic cobalt during humid FTS operation. Despite not observing the agglomerated oxidic cobalt phase, the platinum-promoted catalyst contains much more oxidized cobalt at RH = 57%, compared to the non-promoted sample. From the significantly lower H.F. of the bulk metallic phase for the CoPt/P90 catalyst of 302 kOe compared to the one for Co/P90 of 310 kOe measured at 200 °C, we can infer that the metallic cobalt particles are smaller in CoPt/P90, even after this high humidity treatment. Smaller metallic particles are known to be thermodynamically more susceptible to oxidation than larger ones [77], which helps explaining that, despite the

Table 3
Contribution of the different cobalt phases as determined from MES spectra recorded at 200 °C under varying FTS conditions.

Treatment	H_2O/H_2	Spectral contribution cobalt (%)			
		Co/P90		CoPt/P90	
		Co^0	Co-oxide	Co^0	Co-oxide
Reduced[a]	0	49	51	71	29
RH 0%	0	64	36	63	37
RH 7.5%	0.25	60	40	58	42
RH 14%	0.50	58	42	55	45
RH 20%	0.75	57	43	55	45
RH 25%	1.0	56	44	54	46
Reduced[a]	0	79	21	81	19
RH 0%	0	74	26	71	29
RH 57%	1.0	65	24 / 11	54	46

[a] Reduced spectra were recorded at room temperature.

presence of the reduction promotor, more oxidic cobalt is formed at high humidity. Additionally, smaller metallic particles are also more likely to have a stronger interaction with the titania support, which under reducing conditions results in increased TiO_x overlayer formation, as previously observed for the GP350 catalyst. Formation of such overlayers anchors the cobalt more strongly, which matches our observation of the absence of Co^{3+} species on both CoPt/P90 and Co/GP350. Consequently, the high cobalt-titania interaction results in suppressed sintering but facilitates cobalt oxidation. So, whilst platinum improves cobalt dispersion and results in high cobalt reducibility, further investigation is required in formulating titania-based catalysts that can withstand high steam pressures during operation.

3.6. Catalyst testing

The performance of the cobalt catalysts was measured in a high-pressure fixed-bed plug-flow reactor at 220 °C, 20 bar, a H_2/CO ratio of 4, and a space velocity of 60 L g_{cat}^{-1} h^{-1}. The corresponding results for fresh and used catalysts are collected in Table 4. The fresh catalysts were reduced at 340 °C for 2 h. The used catalysts retrieved after the in situ MES measurements were re-reduced according to the same procedure. The GP350 supported catalysts were also tested, but no conversion was observed on these systems, even when reduction was prolonged at higher temperatures up to 450 °C. This agrees with the activity measured under in situ MES conditions. As the GP350 support does not contain sulfur from the preparation nor alkali metals as confirmed by XPS, we can exclude poisoning as an explanation. Instead, and as rationalized above, the presence of extensive TiO_x overlayers blocks most of the cobalt metal active phase, which is in good agreement with both XPS and Mössbauer characterization results. Additionally, preliminary CO-adsorption IR measurements showed that only through a reduction-oxidation-reduction (ROR) cycle, we could re-expose metallic cobalt. The application of ROR cycles has been reported to remove the titania overlayers formed during reduction [13,29,78,79], thereby uncovering parts of the metallic cobalt surface for CO adsorption. ROR treatments were, however, not possible to perform in the current FT reactor but would be relevant to explore in the future.

For the other catalysts based on P25 and P90, the CTY was in the range of 1.2–3.7 10^{-5} mol_{CO} g_{Co}^{-1} s^{-1} for the freshly reduced and used catalysts. The Co/P90 catalytic activity reported here was obtained after significant time on stream due to technical problems with the GC detector. As the time on stream was extended, we observed an increase in CO conversion, we suspect this is due to further reduction of cobalt, which was found to be difficult through MES and XPS. Due to this extended treatment, the final conversion obtained on this sample is substantially higher than intended, above 10%. As such, the higher CO conversion for this sample makes comparison of the product distribution less meaningful, although no significant differences are observed between the fresh and used Co/P90 catalysts. We can however compare the CTY, which is found to be significantly higher for Co/P90 compared to Co/P25, due to the enhanced cobalt dispersion. This improved activity is even more pronounced when comparing the used catalysts. For both Co/P25 and Co/P90, a decrease in catalytic activity is observed between the freshly reduced and used state, which is caused by sintering of metallic cobalt. This effect is however less pronounced for the Co/P90 catalyst as followed amongst others from the STEM-EDX data. These catalytic activity results show the promise of the P90 titania as a relevant support system for Fischer-Tropsch operations, as it displays improved activity due to the enhanced dispersion of the metallic cobalt and shows lower deactivation between the fresh and spent catalyst, because the stronger titania-cobalt interaction limits extensive sintering.

Besides activity measured on the fresh and spent catalysts, the catalytic activity was also measured in situ during the Mössbauer experiments. This data is provided in Fig. 6 and Table S11. The water-gas shift selectivity was between 0.3% for all catalysts when the RH was 25% or lower and increased to 2–3% for the 57% RH test condition. The introduction of steam to the reactor feed results in a small decrease of

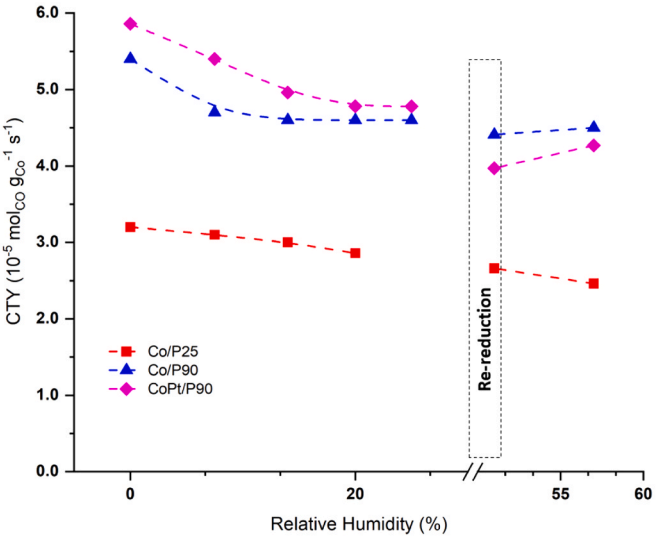

Fig. 6. In situ FTS activity of the Co(Pt)/TiO_2 catalysts during humid FTS measurements in the Mössbauer cell. The CTY determined at steady state at the applied conditions is plotted against the RH. (Co/P25: red squares, Co/P90: blue triangles, CoPt/P90: magenta diamonds). Data points in the dashed box reflect activity under RH= 0% conditions following a re-reduction.

Table 4
Catalytic performance data for the cobalt catalysts (plug-flow reactor operated at 220 °C, 20 bar and $H_2/CO = 4$, SV = 60 L g_{cat}^{-1} h^{-1}). *Test results were obtained after three consecutive reduction and FT activity treatments.

Catalyst	Conversion (%)	C_1 selectivity (%)	C_2-C_4 selectivity (%)	C_{5+} selectivity (%)	CTY (10^{-5} mol_{CO} g_{Co}^{-1} s^{-1})
Co/P25	3	7	7	86	2.1
Co/P25 used	1	14	10	76	1.2
Co/P90*	13	9	10	81	3.7
Co/P90 used	4	8	7	85	2.8
Co/GP350	0	0	0	0	0

the CO and H_2 partial pressures. Subsequently, at the high humidity conditions (RH = 57%), the removal of inert results in an increase of the CO and H_2 partial pressure, which both affect the catalytic activity due to the negative reaction order in CO and the positive order in H_2 [80,81]. As such, these data allow only for a qualitative comparison of the catalytic performance of the various samples.

The activity rates observed for the Co/GP350 catalysts were very low, around 4×10^{-6} mol_{CO} g_{Co}^{-1} s^{-1}, an order of magnitude below the other catalytic samples, which is in agreement with the results shown previously in the PFR reactor. The other catalysts show very similar deactivation profiles in terms of a slow decrease of the catalytic activity with increasing humidity. In the way the experiments are set-up, each humidity step will prolong the Fischer-Tropsch reaction, which will enhance the effect of continuous sintering, as shown previously by Escheman and de Jong [56]. However, the timescales of the two main deactivation pathways relevant for these catalysts are different and we can differentiate both by our experimental procedure. Oxidation is rapid and is only increased when higher humidity conditions are applied, quickly reaching a steady state within the first hours at a given steam partial pressure. Instead, sintering is slow but continuous during a prolonged reaction at given conditions. The effect of sintering can be highlighted by comparing the dry FTS activity following a reduction treatment, which removes all the oxidized cobalt.

The lowest activity, if we disregard the Co/GP350 outlier, was seen for Co/P25 between 2.5 and 3.2 $x\ 10^5$ mol_{CO} g_{Co}^{-1} s^{-1}. The use of the higher titania surface area P90 support resulted in 70–80% higher performance with activity levels between 4.5 and 5.4 $x\ 10^5$ mol_{CO} g_{Co}^{-1} s^{-1}, which was also observed in the ex situ activity measurements discussed above. Interestingly, the use of the P90 support also showed a significant increase in the C_{5+} selectivity compared to the conventional P25 titania catalyst, which coincides with a decrease in the methane selectivity. For both the Co/P25 and Co/P90 catalysts, a decrease in dry FTS activity is observed after re-reduction following the treatment at RH = 25%, indicated by the data in the dashed box in Fig. 6. This irreversible activity loss could point to deactivation through sintering of the metallic cobalt particles. However, STEM-EDX showed that sintering is much less pronounced on the P90 support compared to the conventional P25. This suggests that there is an additional deactivation mechanism resulting in this activity loss, and we believe this is the formation of TiO_x overlayers as also observed on the GP350 catalyst and extensively discussed. Since the P90 support has similar chemistry to the P25, containing both rutile and anatase titania, and the surface area is significantly lower than that of the pure anatase GP350 support, the effect of TiO_x overlayers on P90 is less severe but still observed in situ. The deactivation through overlayers on P90 was not observed in ex situ activity and highlights the importance of measuring in situ and *operando* characterization. The passivation and transfer of the spent sample from the Mössbauer cell and subsequent reduction in the PFR reactor likely acted as a ROR procedure, removing the titania overlayers that formed at high humidity and showing less deactivation during the ex situ activity measurements as a result.

When looking at the addition of platinum on the P90 support, we observe that the activity is similar to the non-promoted catalyst. Nevertheless, the selectivity towards long-chain hydrocarbons is lower, which points to a higher cobalt dispersion in the presence of the promoter, which is in agreement with our Mössbauer and XPS analysis. However, whilst the catalyst is initially more active, the platinum-promoted catalyst shows, after re-reduction, a lower activity compared to its non-promoted counterpart. Under these conditions, the platinum promoted catalyst shows a lower H.F. of 319 kOe compared to 322 kOe for the non-promoted sample, suggesting that the difference is not the result of extensive sintering. Instead, we argue that the improved dispersion of metallic cobalt leads to stronger interaction of cobalt with the titania support, resulting in more extensive TiO_x overlayer formation and less metallic cobalt being accessible for catalysis following the additional reduction treatment. When comparing the activity under dry FTS conditions following to full treatment and the same TOS, the platinum-promoted catalyst has lost 39% of its initial activity (5.9–3.6 $x\ 10^5$ mol_{CO} g_{Co}^{-1} s^{-1}) and the non-promoted catalyst has only lost 19% of its initial activity (5.4–4.4 $x\ 10^5$ mol_{CO} g_{Co}^{-1} s^{-1}). So, whilst the addition of platinum as a FTS promoter offers higher reducibility and enhanced cobalt dispersion, i.e., factors that both increase initial catalyst activity, the catalyst becomes more prone to deactivation at high humidity (RH > 25%). Further investigation is required to reduce this susceptibility to deactivation through TiO_x overlayers and cobalt oxidation.

4. Conclusion

By combining in situ Mössbauer spectroscopy with ex situ characterization, we showed that reduction of a calcined cobalt on titania is hindered by a higher surface area of the titania support. On P90 and GP350 that have a higher surface area than the common P25 titania support, the increased cobalt-titania interactions result in significantly lower cobalt reduction. In situ Mössbauer spectroscopy demonstrated partial oxidation of metallic cobalt under humid FTS conditions for Co/P90 as was earlier found for Co/P25. There was no correlation between the extent of cobalt oxidation and the surface area of the titania support. The low reduction degree of cobalt in Co/GP350, which may also be related to TiO_x overlayer formation, resulted in a negligible FTS activity. Although cobalt reduction in Co/P90 was also lower than in Co/P25, the cobalt mobility on Co/P90 was suppressed, resulting in less cobalt sintering during FTS operation. Promotion of Co/P90 with platinum led to a higher DOR and a higher catalytic performance. However, despite the addition of the platinum promoter, oxidation occurred under high humid FTS conditions. Deactivation was even more significant in this case, which is due to the stronger interaction of dispersed metallic cobalt with the titania support. Nevertheless, compared to P25 the use of P90 with a higher surface area is promising for stably dispersing cobalt with an improved catalytic performance in the FTS reaction.

CRediT authorship contribution statement

Luke van Koppen: Investigation, Data curation, Visualization, Writing- Original draft preparation, Iulian Dugulan: Supervision, Resources, Emiel Hensen: Conceptualization, Supervision, Writing-Reviewing and Editing, Leendert Bezemer: Conceptualization, Funding acquisition, Writing- Reviewing and Editing.

Declaration of Competing Interest

We declare that the submitted work has not been published previously, that it is not under consideration for publication elsewhere, that its publication is approved by all authors and tacitly or explicitly by the responsible authorities where the work was carried out, and that, if accepted, it will not be published elsewhere in the same form, in English or in any other language, including electronically without the written consent of the copyright-holder.

Data Availability

Data will be made available on request.

Acknowledgements

Luke van Koppen acknowledges the financial support from Shell Global Solutions International B.V. The authors thank Dr. Mengyue Wu from Kavli Institute at TU Delft for assistance with STEM-EDX experiments.

Supporting Information

Experimental conditions, Mössbauer fit parameters, Mössbauer

spectra, Ti 2p and Co 2p XPS spectra and discussion of high temperature XPS reduction, XRD, in situ MES catalytic activity, and CO-adsorption FTIR.

Appendix A. Supporting information

Supplementary data associated with this article can be found in the online version at doi:10.1016/j.cattod.2023.114471.

References

[1] M.E. Dry, The Fischer-Tropsch process: 1950-2000, Catal. Today vol. 71 (3–4) (2002) 227–241, https://doi.org/10.1016/S0920-5861(01)00453-9.

[2] G. Maschio, A. Lucchesi, G. Stoppato, Production of syngas from biomass, Bio. Tech. vol. 48 (2) (1994) 119–126, https://doi.org/10.1016/0960-8524(94)90198-8.

[3] K. Zhao, Q. Bkour, X. Hou, S.W. Kang, J.C. Park, M.G. Norton, J.-I. Yang, S. Ha, Reverse water gas shift reaction over CuFe/Al2O3 catalyst in solid oxide electrolysis cell, Chem. Eng. J. vol. 336 (2018) 20–27, https://doi.org/10.1016/j.cej.2017.11.028.

[4] A. de Klerk, Fischer-Tropsch Process. in Kirk-Othmer Encyclopedia of Chemical Technology, Hoboken, John Wiley & Sons, Inc, NJ, USA, 2013, https://doi.org/10.1002/0471238961.fiscdekl.a01.

[5] E. de Smit, B.M. Weckhuysen, The renaissance of iron-based Fischer–Tropsch synthesis: on the multifaceted catalyst deactivation behaviour, Chem. Soc. Rev. vol. 37 (12) (2008) 2758, https://doi.org/10.1039/b805427d.

[6] E. Iglesia, Design, synthesis, and use of cobalt-based Fischer-Tropsch synthesis catalysts, Appl. Catal. A Gen. vol. 161 (1–2) (1997) 59–78, https://doi.org/10.1016/S0926-860X(97)00186-5.

[7] E. Rytter, N.E. Tsakoumis, A. Holmen, On the selectivity to higher hydrocarbons in co-based Fischer-Tropsch synthesis, Catal. Today vol. 261 (2016) 3–16, https://doi.org/10.1016/j.cattod.2015.09.020.

[8] P.J. van Berge, R.C. Everson, Cobalt as an alternative Fischer-Tropsch catalyst to iron for the production of middle distillates, *Stud. Surf. Sci. Catal.* (1997) 207–212, https://doi.org/10.1016/S0167-2991(97)80336-9.

[9] S. Drünert, U. Neuling, T. Zitscher, M. Kaltschmitt, Power-to-Liquid fuels for aviation – processes, resources and supply potential under German conditions, Appl. Energy vol. 277 (2020), 115578, https://doi.org/10.1016/j.apenergy.2020.115578.

[10] G.L. Bezemer, J.H. Bitter, H.P.C.E. Kuipers, H. Oosterbeek, J.E. Holewijn, X. Xu, F. Kapteijn, A.J. van Dillen, K.P. de Jong, Cobalt particle size effects in the Fischer−Tropsch reaction studied with carbon nanofiber supported catalysts, J. Am. Chem. Soc. vol. 128 (12) (2006) 3956–3964, https://doi.org/10.1021/ja058282w.

[11] J.P. den Breejen, P.B. Radstake, G.L. Bezemer, J.H. Bitter, V. Frøseth, A. Holmen, K. P. de Jong, On the origin of the cobalt particle size effects in Fischer−Tropsch catalysis, J. Am. Chem. Soc. vol. 131 (20) (2009) 7197–7203, https://doi.org/10.1021/ja901006x.

[12] N.E. Tsakoumis, M. Rønning, Ø. Borg, E. Rytter, A. Holmen, Deactivation of cobalt based Fischer-Tropsch catalysts: a review, Catal. Today vol. 154 (3–4) (2010) 162–182, https://doi.org/10.1016/j.cattod.2010.02.077.

[13] E. Rytter, A. Holmen, Deactivation and regeneration of commercial Type Fischer-Tropsch co-catalysts—a mini-review, Catalysts vol. 5 (2) (2015) 478–499, https://doi.org/10.3390/catal5020478.

[14] C.H. Bartholomew, Mechanisms of catalyst deactivation, Appl. Catal. A Gen. vol. 212 (1–2) (2001) 17–60, https://doi.org/10.1016/S0926-860X(00)00843-7.

[15] V.V. Ordomsky, A. Carvalho, B. Legras, S. Paul, M. Virginie, V.L. Sushkevich, A. Y. Khodakov, Effects of co-feeding with nitrogen-containing compounds on the performance of supported cobalt and iron catalysts in Fischer–Tropsch synthesis, Catal. Today vol. 275 (2016) 84–93, https://doi.org/10.1016/j.cattod.2015.12.015.

[16] W. Ma, G. Jacobs, D.E. Sparks, B. Todic, D.B. Bukur, B.H. Davis, Quantitative comparison of iron and cobalt based catalysts for the Fischer-Tropsch synthesis under clean and poisoning conditions, Catal. Today vol. 343 (2020) 125–136, https://doi.org/10.1016/j.cattod.2019.04.011.

[17] A.H. Lillebø, E. Patanou, J. Yang, E.A. Blekkan, A. Holmen, The effect of alkali and alkaline earth elements on cobalt based Fischer-Tropsch catalysts, Catal. Today vol. 215 (2013) 60–66, https://doi.org/10.1016/j.cattod.2013.03.030.

[18] C.M. Balonek, A.H. Lillebø, S. Rane, E. Rytter, L.D. Schmidt, A. Holmen, Effect of alkali metal impurities on Co-Re catalysts for Fischer-Tropsch synthesis from biomass-derived syngas, Catal. Lett. vol. 138 (1–2) (2010) 8–13, https://doi.org/10.1007/s10562-010-0366-4.

[19] B.M. Weckhuysen, Preface: recent advances in the in-situ characterization of heterogeneous catalysts, Chem. Soc. Rev. vol. 39 (12) (2010) 4557, https://doi.org/10.1039/c0cs90031a.

[20] P.G. Menon, Coke on catalysts-harmful, harmless, invisible and beneficial types, J. Mol. Catal. vol. 59 (2) (1990) 207–220, https://doi.org/10.1016/0304-5102(90)85053-K.

[21] C.H. Bartholomew, Carbon deposition in steam reforming and methanation, Catal. Rev. vol. 24 (1) (1982) 67–112, https://doi.org/10.1080/03602458208079650.

[22] K. Cheng, V. Subramanian, A. Carvalho, V.V. Ordomsky, Y. Wang, A.Y. Khodakov, The role of carbon pre-coating for the synthesis of highly efficient cobalt catalysts for Fischer-Tropsch synthesis, J. Catal. vol. 337 (2016) 260–271, https://doi.org/10.1016/j.jcat.2016.02.019.

[23] W. Chen, T.F. Kimpel, Y. Song, F.-K. Chiang, B. Zijlstra, R. Pestman, P. Wang, E.J. M. Hensen, Influence of carbon deposits on the cobalt-catalyzed Fischer–tropsch reaction: evidence of a two-site reaction model, ACS Catal. vol. 8 (2) (2018) 1580–1590, https://doi.org/10.1021/acscatal.7b03639.

[24] M. Claeys, M.E. Dry, E. van Steen, E. du Plessis, P.J. van Berge, A.M. Saib, D. J. Moodley, In situ magnetometer study on the formation and stability of cobalt carbide in Fischer–Tropsch synthesis, J. Catal. vol. 318 (2014) 193–202, https://doi.org/10.1016/j.jcat.2014.08.002.

[25] M. Wolf, Thermodynamic assessment of the stability of bulk and nanoparticulate cobalt and nickel during dry and steam reforming of methane, RSC Adv. vol. 11 (30) (2021) 18187–18197, https://doi.org/10.1039/D1RA01856F.

[26] M. Claeys, M.E. Dry, E. van Steen, P.J. van Berge, S. Booyens, R. Crous, P. van Helden, J. Labuschagne, D.J. Moodley, A.M. Saib, Impact of process conditions on the sintering behavior of an alumina-supported Cobalt Fischer–Tropsch catalyst studied with an in situ magnetometer, ACS Catal. vol. 5 (2) (2015) 841–852, https://doi.org/10.1021/cs501810y.

[27] G.L. Bezemer, T.J. Remans, A.P. van Bavel, A.I. Dugulan, Direct evidence of water-assisted sintering of cobalt on carbon nanofiber catalysts during simulated Fischer−Tropsch conditions revealed with in situ mössbauer spectroscopy, J. Am. Chem. Soc. vol. 132 (25) (2010) 8540–8541, https://doi.org/10.1021/ja103002k.

[28] L.M. van Koppen, A.I. Dugulan, G.L. Bezemer, E.J.M. Hensen, Sintering and carbidization under simulated high conversion on a cobalt-based Fischer-Tropsch catalyst; manganese oxide as a structural promotor, J. Catal. vol. 413 (2022) 106–118, https://doi.org/10.1016/j.jcat.2022.06.020.

[29] C.E. Kliewer, S.L. Soled, G. Kiss, Morphological transformations during Fischer-Tropsch synthesis on a titania-supported cobalt catalyst, Catal. Today vol. 323 (2019) 233–256, https://doi.org/10.1016/j.cattod.2018.05.021.

[30] D. Kistamurthy, A.M. Saib, D.J. Moodley, J.W. Niemantsverdriet, C.J. Weststrate, Ostwald ripening on a planar Co/SiO 2 catalyst exposed to model Fischer–Tropsch synthesis conditions, *J. Catal.* vol. 328 (2015) 123–129, https://doi.org/10.1016/j.jcat.2015.02.017.

[31] W. Janse Van Rensburg, P. Van Helden, D.J. Moodley, M. Claeys, M.A. Petersen, E. Van Steen, Role of transient co-subcarbonyls in ostwald ripening sintering of cobalt supported on γ-alumina surfaces, J. Phys. Chem. C. vol. 121 (31) (2017) 16739–16753, https://doi.org/10.1021/acs.jpcc.7b01907.

[32] J. van de Loosdrecht, B. Balzhinimaev, J.A. Dalmon, J.W. Niemantsverdriet, S. V. Tsybulya, A.M. Saib, P.J. van Berge, J.L. Visagie, Cobalt Fischer-Tropsch synthesis: deactivation by oxidation? Catal. Today vol. 123 (1–4) (2007) 293–302, https://doi.org/10.1016/j.cattod.2007.02.032.

[33] M. Wolf, B.K. Mutuma, N.J. Coville, N. Fischer, M. Claeys, Role of CO in the water-induced formation of cobalt oxide in a high conversion Fischer–Tropsch Environment, ACS Catal. vol. 8 (5) (2018) 3985–3989, https://doi.org/10.1021/acscatal.7b04177.

[34] M. Wolf, N. Fischer, M. Claeys, Capturing the interconnectivity of water-induced oxidation and sintering of cobalt nanoparticles during the Fischer-Tropsch synthesis in situ, J. Catal. vol. 374 (2019) 199–207, https://doi.org/10.1016/j.jcat.2019.04.030.

[35] E. Rytter, A. Holmen, Perspectives on the effect of water in cobalt Fischer-Tropsch synthesis, ACS Catal. vol. 7 (8) (2017) 5321–5328, https://doi.org/10.1021/acscatal.7b01525.

[36] L.M. van Koppen, A.I. Dugulan, G.L. Bezemer, E.J.M. Hensen, Elucidating deactivation of titania-supported cobalt Fischer-Tropsch catalysts under simulated high conversion conditions, J. Catal. vol. 420 (2023) 44–57, https://doi.org/10.1016/j.jcat.2023.02.019.

[37] Z. Yu, Ø. Borg, D. Chen, B.C. Enger, V. Frøseth, E. Rytter, H. Wigum, A. Holmen, Carbon nanofiber supported cobalt catalysts for fischer–tropsch synthesis with high activity and selectivity, Catal. Lett. vol. 109 (1–2) (2006) 43–47, https://doi.org/10.1007/s10562-006-0054-6.

[38] Ø. Borg, Z. Yu, D. Chen, E.A. Blekkan, E. Rytter, A. Holmen, The effect of water on the activity and selectivity for carbon nanofiber supported cobalt Fischer-Tropsch catalysts, Top. Catal. vol. 57 (6–9) (2014) 491–499, https://doi.org/10.1007/s11244-013-0205-0.

[39] N.E. Tsakoumis, R. Dehghan, R.E. Johnsen, A. Voronov, W. Van Beek, J. C. Walmsley, Ø. Borg, E. Rytter, D. Chen, M. Rønning, A. Holmen, A combined in situ XAS-XRPD-Raman study of Fischer-Tropsch synthesis over a carbon supported Co catalyst, Catal. Today vol. 205 (2013) 86–93, https://doi.org/10.1016/j.cattod.2012.08.041.

[40] A. Carvalho, V.V. Ordomsky, Y. Luo, M. Marinova, A.R. Muniz, N.R. Marcilio, A. Y. Khodakov, Elucidation of deactivation phenomena in cobalt catalyst for Fischer-Tropsch synthesis using SSITKA, J. Catal. vol. 344 (2016) 669–679, https://doi.org/10.1016/j.jcat.2016.11.001.

[41] B. Ernst, S. Libs, P. Chaumette, A. Kiennemann, Preparation and characterization of Fischer–Tropsch active Co/SiO_2 catalysts, Appl. Catal. A Gen. vol. 186 (1–2) (1999) 145–168, https://doi.org/10.1016/S0926-860X(99)00170-2.

[42] A.Y. Khodakov, J. Lynch, D. Bazin, B. Rebours, N. Zanier, B. Moisson, P. Chaumette, Reducibility of cobalt species in silica-supported Fischer-Tropsch catalysts, J. Catal. vol. 168 (1) (1997) 16–25, https://doi.org/10.1006/jcat.1997.1573.

[43] A.Y. Khodakov, A. Griboval-Constant, R. Bechara, V.L. Zholobenko, Pore size effects in fischer tropsch synthesis over cobalt-supported mesoporous silicas, J. Catal. vol. 206 (2) (2002) 230–241, https://doi.org/10.1006/jcat.2001.3496.

[44] J.S. Jung, S.W. Kim, D.J. Moon, Fischer-Tropsch synthesis over cobalt based catalyst supported on different mesoporous silica, Catal. Today vol. 185 (1) (2012) 168–174, https://doi.org/10.1016/j.cattod.2012.02.002.

[45] M. Wolf, H. Kotzé, N. Fischer, M. Claeys, Size dependent stability of cobalt nanoparticles on silica under high conversion Fischer–Tropsch environment, Far. Dis. vol. 197 (2017) 243–268, https://doi.org/10.1039/C6FD00200E.
[46] J.P. den Breejen, A.M. Frey, J. Yang, A. Holmen, M.M. van Schooneveld, F.M.F. de Groot, O. Stephan, J.H. Bitter, K.P. de Jong, A highly active and selective manganese oxide promoted cobalt-on-silica fischer–tropsch catalyst, Top. Catal. vol. 54 (13–15) (2011) 768–777, https://doi.org/10.1007/s11244-011-9703-0.
[47] M. Voß, D. Borgmann, G. Wedler, Characterization of alumina, silica, and titania supported cobalt catalysts, J. Catal. vol. 212 (1) (2002) 10–21, https://doi.org/10.1006/jcat.2002.3739.
[48] E. Rytter, A. Holmen, On the support in cobalt Fischer–Tropsch synthesis—Emphasis on alumina and aluminates, Catal. Today vol. 275 (2016) 11–19, https://doi.org/10.1016/j.cattod.2015.11.042.
[49] J. Wang, P.A. Chernavskii, A.Y. Khodakov, Y. Wang, Structure and catalytic performance of alumina-supported copper-cobalt catalysts for carbon monoxide hydrogenation, J. Catal. vol. 286 (2012) 51–61, https://doi.org/10.1016/j.jcat.2011.10.012.
[50] C. Lancelot, V.V. Ordomsky, O. Stéphan, M. Sadeqzadeh, H. Karaca, M. Lacroix, D. Curulla-Ferré, F. Luck, P. Fongarland, A. Griboval-Constant, A.Y. Khodakov, Direct Evidence of Surface Oxidation of Cobalt Nanoparticles in Alumina-Supported Catalysts for Fischer–Tropsch Synthesis, ACS Catal. vol. 4 (12) (2014) 4510–4515, https://doi.org/10.1021/cs500981p.
[51] H. Karaca, J. Hong, P. Fongarland, P. Roussel, A. Griboval-Constant, M. Lacroix, K. Hortmann, O.V. Safonova, A.Y. Khodakov, In situ XRD investigation of the evolution of alumina-supported cobaltcatalysts under realistic conditions of Fischer-Tropsch synthesis, Chem. Commun. vol. 46 (5) (2010) 788–790, https://doi.org/10.1039/B920110F.
[52] H. Karaca, O.V. Safonova, S. Chambrey, P. Fongarland, P. Roussel, A. Griboval-Constant, M. Lacroix, A.Y. Khodakov, Structure and catalytic performance of Pt-promoted alumina-supported cobalt catalysts under realistic conditions of Fischer–Tropsch synthesis, J. Catal. vol. 277 (1) (2011) 14–26, https://doi.org/10.1016/j.jcat.2010.10.007.
[53] A. Rochet, V. Moizan, F. Diehl, C. Pichon, V. Briois, Quick-XAS and Raman operando characterization of a cobalt alumina-supported catalyst under realistic Fischer-Tropsch reaction conditions, Catal. Today vol. 205 (2013) 94–100, https://doi.org/10.1016/j.cattod.2012.08.021.
[54] M. Sadeqzadeh, S. Chambrey, J. Hong, P. Fongarland, F. Luck, D. Curulla-Ferré, D. Schweich, J. Bousquet, A.Y. Khodakov, Effect of different reaction conditions on the deactivation of alumina-supported cobalt Fischer-Tropsch catalysts in a milli-fixed-bed reactor: Experiments and modeling, Ind. Eng. Chem. Res. vol. 53 (17) (2014) 6913–6922, https://doi.org/10.1021/ie4040303.
[55] E. Rytter, Ø. Borg, N.E. Tsakoumis, A. Holmen, Water as key to activity and selectivity in Co Fischer-Tropsch synthesis: γ-alumina based structure-performance relationships, J. Catal. vol. 365 (2018) 334–343, https://doi.org/10.1016/j.jcat.2018.07.003.
[56] T.O. Eschemann, K.P. de Jong, Deactivation Behavior of Co/TiO_2 Catalysts during Fischer–Tropsch Synthesis, ACS Catal. vol. 5 (6) (2015) 3181–3188, https://doi.org/10.1021/acscatal.5b00268.
[57] T.O. Eschemann, J. Oenema, K.P. de Jong, Effects of noble metal promotion for Co/TiO_2 Fischer-Tropsch catalysts, Catal. Today vol. 261 (2016) 60–66, https://doi.org/10.1016/j.cattod.2015.06.016.
[58] T.O. Eschemann, J.H. Bitter, K.P. De Jong, Effects of loading and synthesis method of titania-supported cobalt catalysts for Fischer-Tropsch synthesis, Catal. Today vol. 228 (2014) 89–95, https://doi.org/10.1016/j.cattod.2013.10.041.
[59] F. Morales, D. Grandjean, F.M.F. de Groot, O. Stephan, B.M. Weckhuysen, Combined EXAFS and STEM-EELS study of the electronic state and location of Mn as promoter in Co-based Fischer–Tropsch catalysts, Phys. Chem. Chem. Phys. vol. 7 (4) (2005) 568–572, https://doi.org/10.1039/B418286C.
[60] F. Morales, D. Grandjean, A. Mens, F.M.F. de Groot, B.M. Weckhuysen, X-ray absorption spectroscopy of Mn/Co/TiO_2 Fischer−Tropsch catalysts: relationships between preparation method, molecular structure, and catalyst performance, J. Phys. Chem. B vol. 110 (17) (2006) 8626–8639, https://doi.org/10.1021/jp0565958.
[61] F. Morales, F.M.F. De Groot, P. Glatzel, E. Kleimenov, H. Bluhm, M. Hävecker, A. Knop-Gericke, B.M. Weckhuysen, In situ X-ray absorption of Co/Mn/TiO 2 catalysts for Fischer-Tropsch synthesis, J. Phys. Chem. B vol. 108 (41) (2004) 16201–16207, https://doi.org/10.1021/jp0403846.
[62] S.J. Tauster, S.C. Fung, R.L. Garten, Strong metal-support interactions. Group 8 noble metals supported on titanium dioxide, J. Am. Chem. Soc. vol. 100 (1) (1978) 170–175, https://doi.org/10.1021/ja00469a029.
[63] S.J. Tauster, S.C. Fung, R.T.K. Baker, J.A. Horsley, Strong interactions in supported-metal catalysts, Science vol. 211 (4487) (1981) 1121–1125, https://doi.org/10.1126/science.211.4487.1121.
[64] M. Wolf, N. Fischer, M. Claeys, Water-induced deactivation of cobalt-based Fischer–Tropsch catalysts, Nat. Catal. vol. 3 (12) (2020) 962–965, https://doi.org/10.1038/s41929-020-00534-5.
[65] M. Wolf, E.K. Gibson, E.J. Olivier, J.H. Neethling, C.R.A. Catlow, N. Fischer, M. Claeys, In-depth characterization of metal-support compounds in spent Co/SiO_2 Fischer-Tropsch model catalysts, Catal. Today vol. 342 (2020) 71–78, https://doi.org/10.1016/j.cattod.2019.01.065.
[66] M. Wolf, E.K. Gibson, E.J. Olivier, J.H. Neethling, C.R.A. Catlow, N. Fischer, M. Claeys, Water-induced formation of cobalt-support compounds under simulated high conversion Fischer–Tropsch environment, ACS Catal. vol. 9 (6) (2019) 4902–4918, https://doi.org/10.1021/acscatal.9b00160.
[67] M.W.J. Crajé, A.M. Van der Kraan, J. Van de Loosdrecht, P.J. Van Berge, The application of Mössbauer emission spectroscopy to industrial cobalt based Fischer-Tropsch catalysts, Catal. Today vol. 71 (3–4) (2002) 369–379, https://doi.org/10.1016/S0920-5861(01)00464-3.
[68] Z. Klencsár, MossWinn—methodological advances in the field of Mössbauer data analysis, Hyperfine Inter. vol. 217 (1–3) (2013) 117–126, https://doi.org/10.1007/s10751-012-0732-2.
[69] J.A. Tjon, M. Blume, Mössbauer spectra in a fluctuating environment ii. randomly varying electric field gradients, Phys. Rev. vol. 165 (2) (1968) 456–461, https://doi.org/10.1103/PhysRev.165.456.
[70] T. Ohno, K. Sarukawa, K. Tokieda, M. Matsumura, Morphology of a TiO_2 photocatalyst (Degussa, P-25) consisting of anatase and rutile crystalline phases, J. Catal. vol. 203 (1) (2001) 82–86, https://doi.org/10.1006/jcat.2001.3316.
[71] T. A Dontsova, O.I. Yanushevska, S.V. Nahirniak, A.S. Kutuzova, G.V. Krymets, P. S. Smertenko, Characterization of commercial TiO_2 P90 modified with ZnO by the impregnation method, J. Chem., Vol. 2021 (2021) 1–11, https://doi.org/10.1155/2021/9378490.
[72] A. Desmartin-Chomel, J.L. Flores, A. Bourane, J.M. Clacens, F. Figueras, G. Delahay, A.G. Fendler, C. Lehaut-Burnouf, Calorimetric and FTIR study of the acid properties of sulfated titanias, J. Phys. Chem. B vol. 110 (2) (2006) 858–863, https://doi.org/10.1021/jp0530698.
[73] M.C. Biesinger, B.P. Payne, A.P. Grosvenor, L.W.M. Lau, A.R. Gerson, R. St, C. Smart, Resolving surface chemical states in XPS analysis of first row transition metals, oxides and hydroxides: Cr, Mn, Fe, Co and Ni, Appl. Surf. Sci. vol. 257 (7) (2011) 2717–2730, https://doi.org/10.1016/j.apsusc.2010.10.051.
[74] T.W. van Deelen, J.J. Nijhuis, N.A. Krans, J. Zečević, K.P. de Jong, Preparation of cobalt nanocrystals supported on metal oxides to study particle growth in fischer–tropsch catalysts, ACS Catal. vol. 8 (11) (2018) 10581–10589, https://doi.org/10.1021/acscatal.8b03094.
[75] C. Wivel, B.S. Clausen, R. Candia, S. Mørup, H. Topsøe, Mössbauer emission studies of calcined Co-Mo/Al_2O_3 catalysts: catalytic significance of Co precursors, J. Catal. vol. 87 (2) (1984) 497–513, https://doi.org/10.1016/0021-9517(84)90210-0.
[76] M. Monai, et al., Restructuring of titanium oxide overlayers over nickel nanoparticles during catalysis, Science vol. 380 (6645) (2023) 644–651, https://doi.org/10.1126/science.adf6984.
[77] H.J. Lipkin, Some simple features of the Mossbauer effect, Ann. Phys. (N. Y) vol. 18 (2) (1962) 182–197, https://doi.org/10.1016/0003-4916(62)90066-0.
[78] J.H. Den Otter, S.R. Nijveld, K.P. De Jong, Synergistic promotion of Co/SiO_2 fischer-tropsch catalysts by niobia and platinum, ACS Catal. vol. 6 (3) (2016) 1616–1623, https://doi.org/10.1021/acscatal.5b02418.
[79] A.M. Saib, D.J. Moodley, I.M. Ciobîc, M.M. Hauman, B.H. Sigwebela, C. J. Weststrate, J.W. Niemantsverdriet, J. Van De Loosdrecht, Fundamental understanding of deactivation and regeneration of cobalt Fischer-Tropsch synthesis catalysts, Catal. Today vol. 154 (3–4) (2010) 271–282, https://doi.org/10.1016/j.cattod.2010.02.008.
[80] W. Chen, R. Pestman, B. Zijlstra, I.A.W. Filot, E.J.M. Hensen, Mechanism of cobalt-catalyzed CO hydrogenation: 1. methanation, ACS Catal. vol. 7 (12) (2017) 8050–8060, https://doi.org/10.1021/acscatal.7b02757.
[81] R. Pestman, W. Chen, E. Hensen, Insight into the rate-determining step and active sites in the fischer–tropsch reaction over cobalt catalysts, ACS Catal. vol. 9 (5) (2019) 4189–4195, https://doi.org/10.1021/acscatal.9b00185.